Propagation of medium scale traveling ionospheric disturbances at different latitudes and solar cycle conditions

M. Hernández-Pajares,[1] J. M. Juan,[1] J. Sanz,[1] and A. Aragón-Àngel[1,2]

Received 2 December 2011; revised 6 April 2012; accepted 1 May 2012; published 4 July 2012.

[1] In this work, an extension in latitude range and time span with respect previous studies on Medium Scale Traveling Ionospheric Disturbances (MSTID) propagation, is presented. So far they have been basically studied at mid latitude and for limited periods (less than few years) at solar maximum conditions. This extension has been possible due to the availability of local Global Positioning System (GPS) networks at mid-north hemisphere (California), mid-south hemisphere (New Zealand), high and low latitudes (Alaska and Hawaii), for the last 13, 11, 7 and 4 years respectively. Optimal algorithms specially suitable for mass data processing have been used, such as the Single Receiver Medium Scale Traveling Ionospheric activity index (SRMTID) and the phase difference method for MSTID propagation estimation. The results reveal that several of the main MSTID climatological trends at mid latitude are also shared at low and high latitude, also modulated in intensity also by the Solar Cycle. This is the case for local fall/winter day-time equatorward propagated MSTIDs with typical velocities and wavelengths of 150–250 m/s and 100–300 km respectively. Moreover the comparison of MSTID propagation estimation using different techniques, and their implications in terms of potential origins of MSTIDs, are also discussed.

Citation: Hernández-Pajares, M., J. M. Juan, J. Sanz, and A. Aragón-Àngel (2012), Propagation of medium scale traveling ionospheric disturbances at different latitudes and solar cycle conditions, *Radio Sci.*, *47*, RS0K05, doi:10.1029/2011RS004951.

1. Introduction

[2] The MSTIDs are ionospheric signatures of waves, up to few TECUs of amplitude in solar cycle maximum conditions (1 TECU = $10^{16}e^{-}/m^{3}$), which propagate with typical periods ranging from several minutes to less than one hour, and velocities from 50 to 300 m/s (see for instance *Hunsucker* [1982], *Tsugawa et al.* [2007], and *Hernández-Pajares et al.* [2006a] (hereinafter HJS06) and an illustrative example in Figure 1). In spite of some authors using the MSTID term to refer only to a subset of them (those occurring during night and local winter and moving westward with not a clear origin [see *Kelley*, 2011]), we will keep the original scope for the MSTID term, which includes all of ionospheric wave signatures fitting in the aforementioned range of velocities and periods. In particular, MSTIDs occurring at local day time and winter, moving equatorward, which seem to be due to classical Atmospheric Gravity Wave (AGW) interaction with the ionosphere [*Kelley*, 2011], are also considered in such term.

[3] Different techniques and applications are sensitive to the MSTIDs effect at mid latitudes, appearing as small ionospheric electron content gradients (up to few TECU) at length scales of half MSTID wavelengths (typically ranging from 50 to 300 km, see for instance HJS06). This effect frequently occurs due to the above mentioned MSTID systematic occurrence on a seasonal basis (during fall/winter mainly at day time versus spring/summer at nighttime as it will be confirmed in this work), and therefore necessary to be modeled and mitigated. One example of these affected techniques where the knowledge of MSTID characteristics matters is precise GNSS positioning [see *Coster and Tsugawa*, 2008; *Hernández-Pajares et al.*, 2006b]. In the latter a simple propagation model, deduced from old observations, significantly reduces (up to 50%) the error of Real Time Kinematic (RTK) and Wide Area RTK GPS navigation, maintaining the decimeter-error positioning even under strong MSTID activity. Measurements from other sources that can be affected by MSTIDs are those of radio astronomy, in particular from the Very Large Base Interferometry technique [see, e.g., *Frey et al.*, 2003; *Watts et al.*, 2010; *Thompson et al.*, 2001].

[4] The origin of Traveling Ionospheric Disturbances (TIDs) is not well established yet, but several potential sources have been pointed out [see, e.g., *Scotto*, 1995; *Kelley*, 2011]:

[5] 1. The auroral zone, in terms of Lorentz force and Joule dissipation associated to particle precipitation [see, e.g., *Hunsucker*, 1982]. This potential source seems to be associated to Large Scale TIDs (LSTIDs), with wavelengths of

[1]Research Group of Astronomy and Geomatics, Universitat Politècnica de Catalunya, Barcelona, Spain.
[2]gAGE-NAV S.L., Barcelona, Spain.

Corresponding author: M. Hernández-Pajares, Research Group of Astronomy and Geomatics, Universitat Politècnica de Catalunya, ES-08034 Barcelona, Spain. (manuel@ma4.upc.edu)

0048-6604/12/2011RS004951

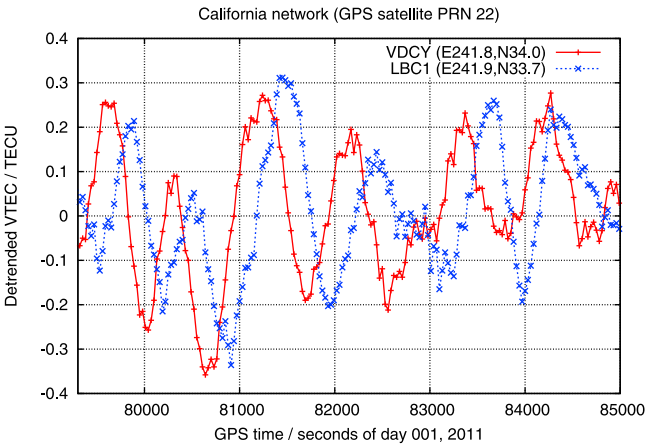

Figure 1. Example of MSTID signature in the detrended VTEC, directly obtained from the ionospheric combination of GPS carrier phases (see section 3) corresponding to an MSTID affecting GPS satellite PRN 22, advancing from receiver VDCY (E241.8,N34.0) toward LBC1 (E241.9, N33.7) in California network (CA, January 1st, 2011, see Figure 19 for more details).

about 1000 km and velocities of 400–1000 m/s and out of the scope of this work.

[6] 2. The neutral atmosphere turbulence associated to meteorological activity and atmospheric winds. However, this is not a clear candidate to account for the repeatability of MSTIDs, following *Scotto* [1995].

[7] 3. The vertical irradiance gradient associated to the Solar Terminator (ST) at the given ionospheric region and its magnetic conjugate region, which seems to be a solid candidate to explain most part of the MSTID climatology [see *Afraimovich et al.*, 2009; HJS06].

[8] 4. The Perkins instability, which would make understandable, in terms of the weakest damping direction, the preferred westward propagation of local winter MSTIDs at night [*Kelley*, 2011].

[9] In this context, the contribution of this paper is to increase the knowledge of the characterization of MSTIDs, for high, low and mid latitude, during the longest available period of most recent local GPS network data (from 4 to 13 years), in order to answer the question about the extrapolability of mid latitude MSTID characteristics to high and low latitudes. By studying four dual-frequency GPS local networks at California, New Zealand, Alaska and Hawaii, it will be shown that, in great extent, this is the case. The comparison with recent estimations of MSTID propagation and potential sources will be finally presented and discussed.

[10] The paper is divided in to several sections, presenting the datasets used, the MSTID propagation estimation algorithm, its characteristics and the corresponding discussion of results.

2. Datasets: Representative Local GPS Networks at Different Latitudes

[11] As it is well known, GPS networks of dual-frequency permanent ground receivers have become an excellent ionospheric sounding technique [see, e.g., *Hernández-Pajares et al.*, 2011]: in accuracy (better than 0.1 TECU in Slant Total Electron Content variation); in temporal resolution (simultaneous observations from each receiver of several GPS satellites each 30 s, down to 1 s, typically); and in spatial coverage, from local networks with baselines of several kilometers up to global coverage by means of the International GNSS Service (IGS) network [see *Dow et al.*, 2009].

[12] In order to study the propagation characteristics of MSTID at different latitudes, several local networks, with separations among receivers up to few tens of kilometers to properly detect them (similarly as done in HJS06 for four mid latitude networks), have been identified in one of the largest available existing public GPS data servers, provided

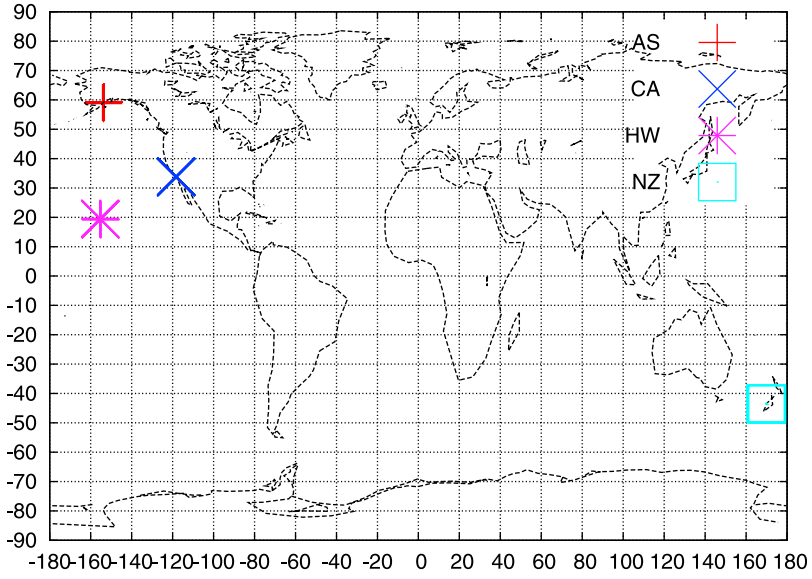

Figure 2. Global location of the local GPS networks analyzed in this work, at South of Alaska (AS), California (CA), Hawaii (HW) and New Zealand (NZ).

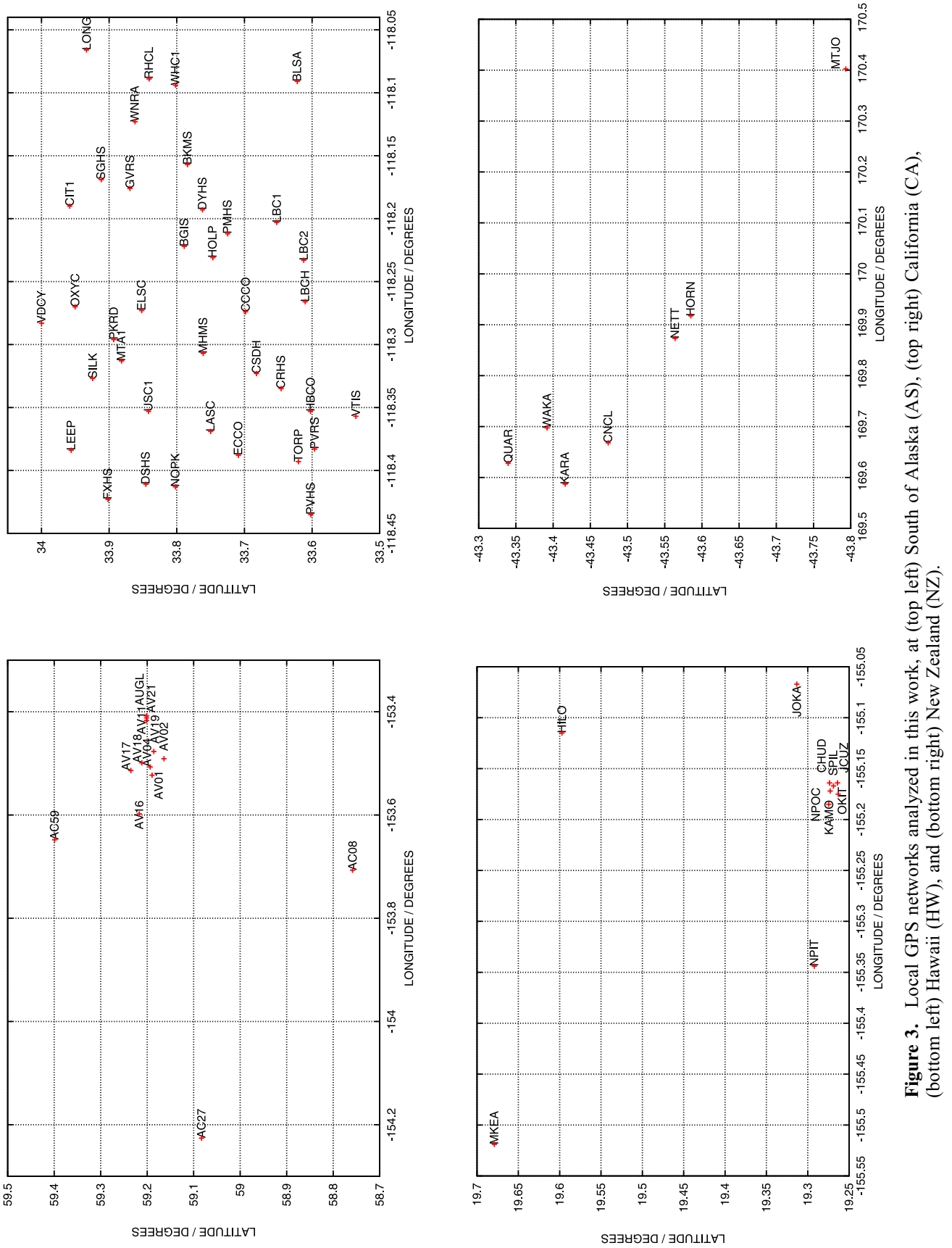

Figure 3. Local GPS networks analyzed in this work, at (top left) South of Alaska (AS), (top right) California (CA), (bottom left) Hawaii (HW), and (bottom right) New Zealand (NZ).

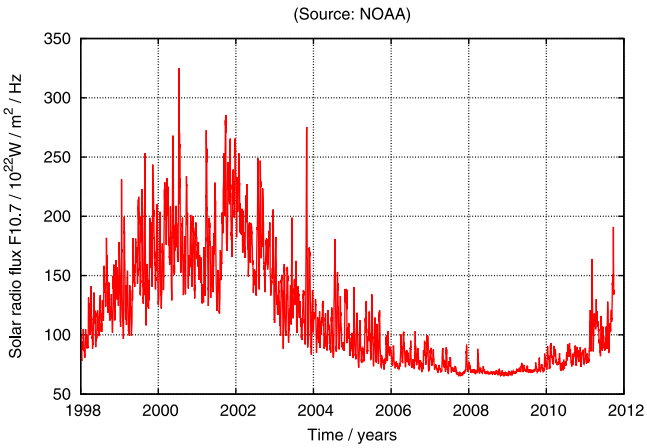

Figure 4. Solar flux during the longest available dataset under study (CA network, since 1998).

by the University of California at San Diego (http://garner.ucsd.edu).

[13] Indeed, four local GPS networks have been selected with available public data, two of them at midlatitude in both hemispheres, at California (CA) and at New Zealand (NZ), one at high latitude (South Alaska, AS) and the last one at low latitude (Hawaii, HW) in order to check whether a common behavior occurs, in terms of both occurrence and propagation, also in Solar Minimum conditions (see Figures 2 and 3, being two of these networks, CA and NZ, coincident with those used in HJS06). A total of up to 13, 38, 10 and 7 receivers have been processed for AS, CA, HW and NZ networks, respectively.

[14] In order to optimally sample the seasonal behavior of MSTIDs during the periods where the corresponding observations are available (the last 7, 13, 4 and 11 years, until September 2011, for AS, CA, HW and NZ respectively, increasing the 3 years of processed data in HJS06), at least one day every two weeks is analyzed, dramatically diminishing the computational and storage requirements to affordable levels (this translates into a total of 204, 373, 117 and 417 processed days with more than 40, 200, 30 and 50 millions dual frequency observations respectively). This fortnightly or higher sampling is enough to study the seasonal MSTID climatology during the last 4–13 years, including the very recent solar minimum and increasing conditions (see corresponding Solar Flux, showing the last solar cycle signature, in Figure 4).

3. Efficient Computation of MSTID Characteristics

[15] The MSTID detection and propagation estimation algorithm has been implemented by updating the one presented in HJS06. Indeed, it is based in the cross-correlation of the detrended Total Electron Content (TEC) values observed for a given GPS satellite within a local network (similarly to HJS06), but directly using the complex phase of the dominant Fourier Transform terms to determine the propagation velocities, instead of the direct cross-correlation of the filtered TEC signals. This allows a significant computation offloading, quite adequate for analyzing vast amounts of data.

3.1. First Band Pass TEC Filtering

[16] One first important issue is to find a sensitive and efficient approach to perform a first band pass filtering, sensitive to the expected spectral region for the MSTIDs, and suitable for processing huge amounts of data. It is used, as in HJS06, the double differences over time of ionospheric (geometric-free) combination L_I ($\delta^2 L_I$) of GPS carrier phases L_1, L_2 ($L_I = L_1 - L_2$ all of them expressed in length units), with a time step (τ) of 300 s. The reason is that, for a given MSTID *mode* of frequency f for the Slant Total Electron Content (Slant TEC or STEC, S),

$$S = A e^{j2\pi f t}, \tag{1}$$

where A is the MSTID mode amplitude, $j = \sqrt{-1}$ is the complex unit and t is the time, and considering the detrended STEC definition, $\tilde{S}$, as:

$$\tilde{S} \equiv S(t) - \frac{1}{2}(S(t+\tau) + S(t-\tau)) = -2\delta^2 S \tag{2}$$

it is easy to demonstrate that $\tilde{S}$ can be expressed (similarly as shown in HJS06) as:

$$\tilde{S} = 2\sin^2(\pi f \tau)\, S \tag{3}$$

where $\tilde{S} = \tilde{L}_I$ if no cycle slip occurs among the three involved measurements [see, e.g., *Hernández-Pajares et al.*, 2011].

[17] In Figure 5 it can be seen that the chosen value of $\tau = 300$ s allows a significant sensibility in the most part of MSTID spectra, above the buoyancy periods -corresponding to the Brunt-Väisälä frequencies- of 600–700 s (see for instance HJS08), and up to 1800 s (amplified up to 1200 s).

3.2. Single Receiver MSTID Activity Index

[18] Once the initial quick filtering is performed, a straightforward undifferenced MSTID activity index can be used: the Single Receiver Medium scale Traveling Ionospheric Disturbance (SRMTID index, already independently

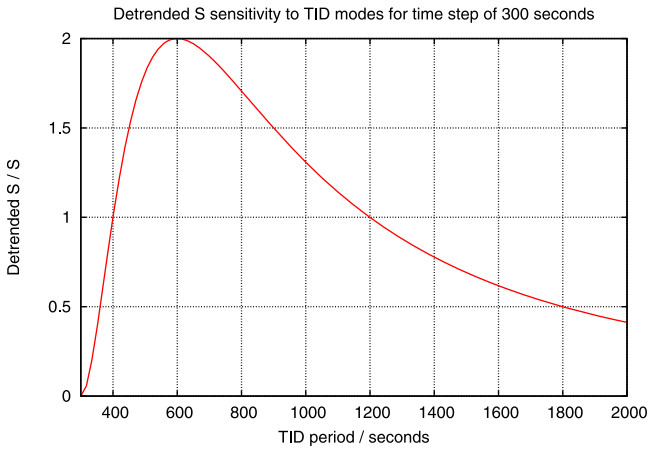

Figure 5. Augmentation factor of the initial mode amplitude ($\tilde{S}/S$), for time step of $\tau = 300$ s, in terms of the MSTID mode period.

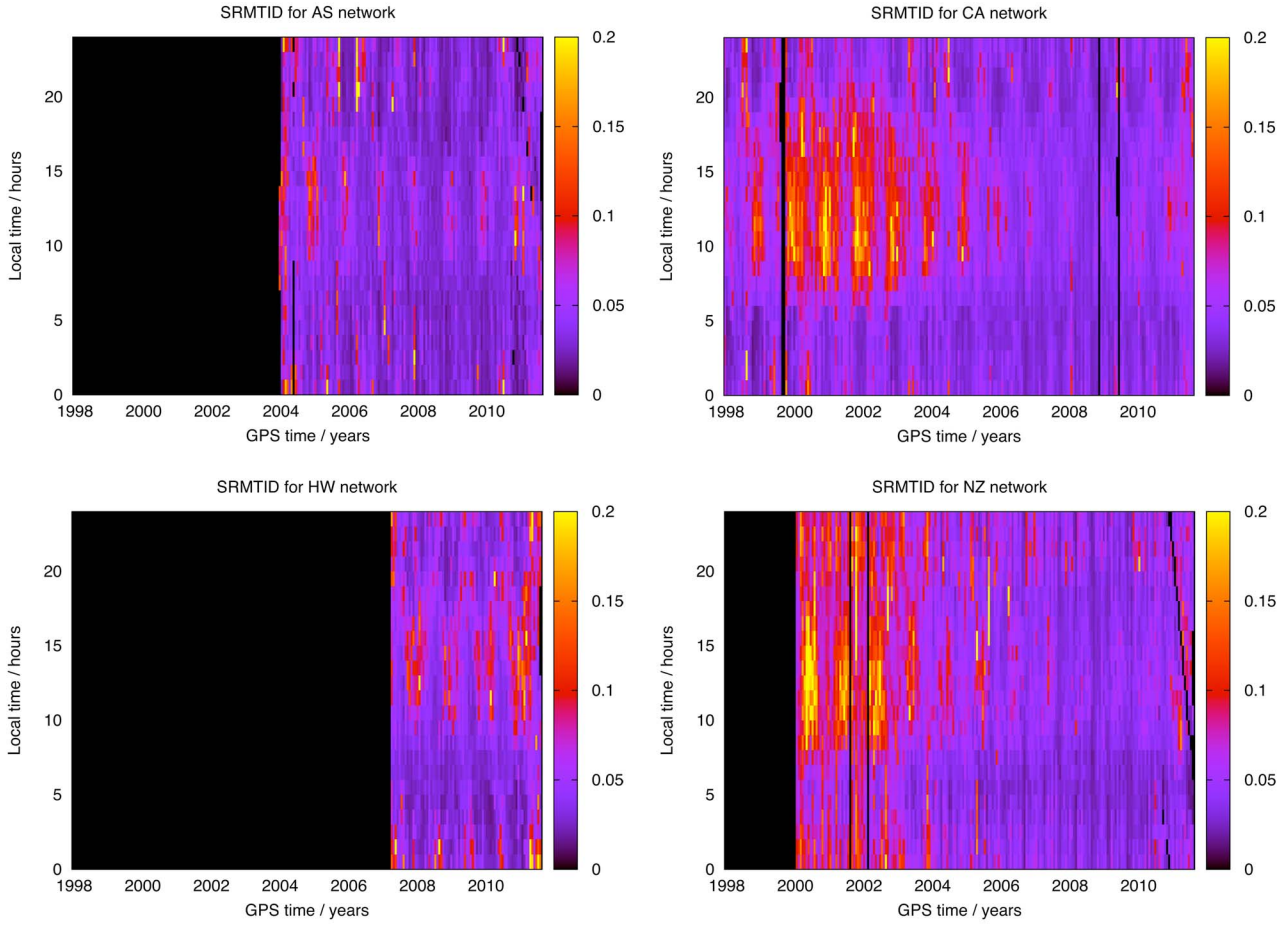

Figure 6. SRMTID index (in TECUs), in terms of GPS time (x-axis) and local time (y-axis), for the four selected networks: (top left) AS, (top right) CA, (bottom left) HW, and (bottom right) NZ.

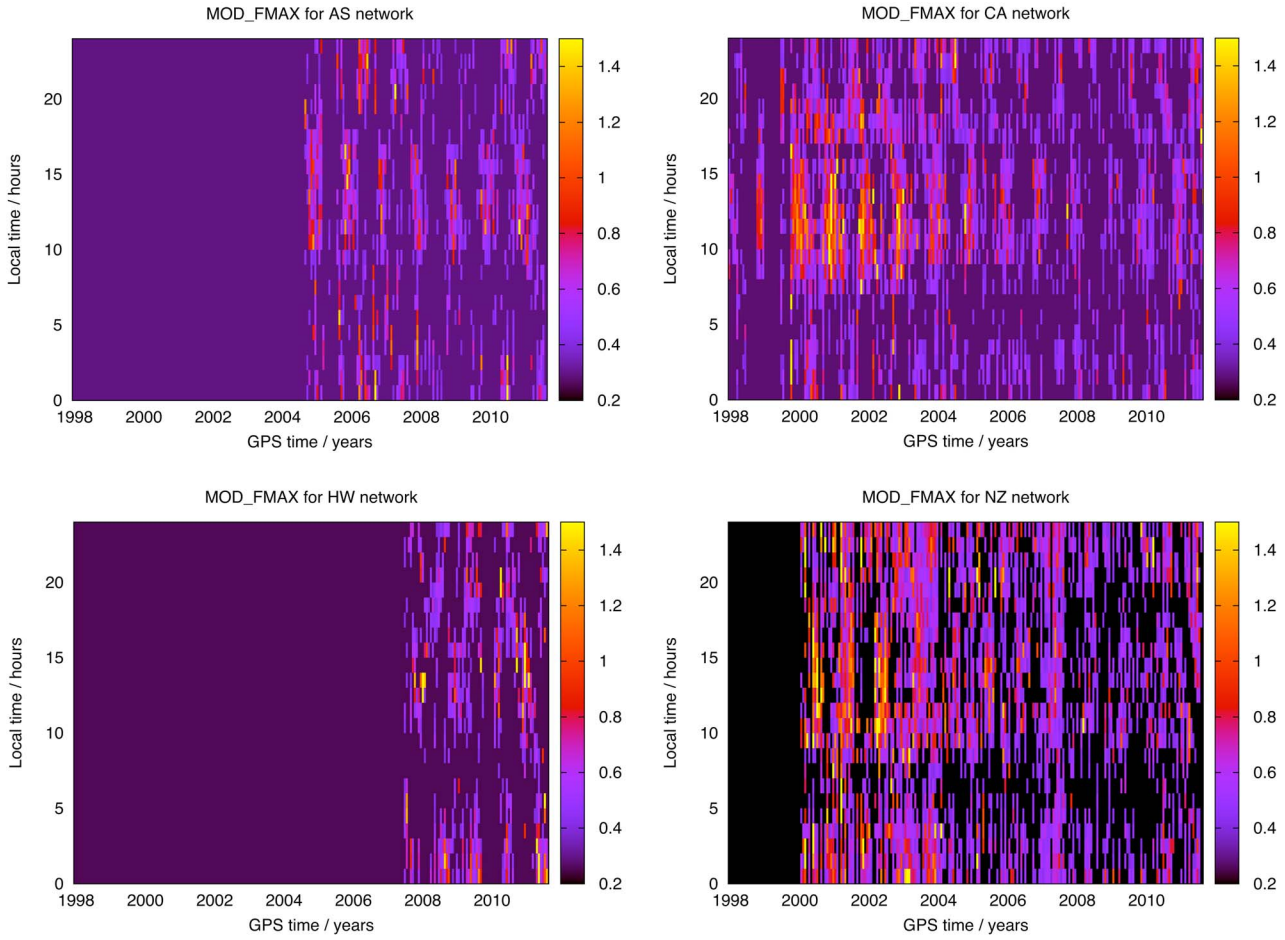

Figure 7. Module of the dominant MSTID frequency (in TECUs), in terms of GPS time (x-axis) and local time (y-axis), for the four selected networks: (top left) AS, (top right) CA, (bottom left) HW, and (bottom right) NZ.

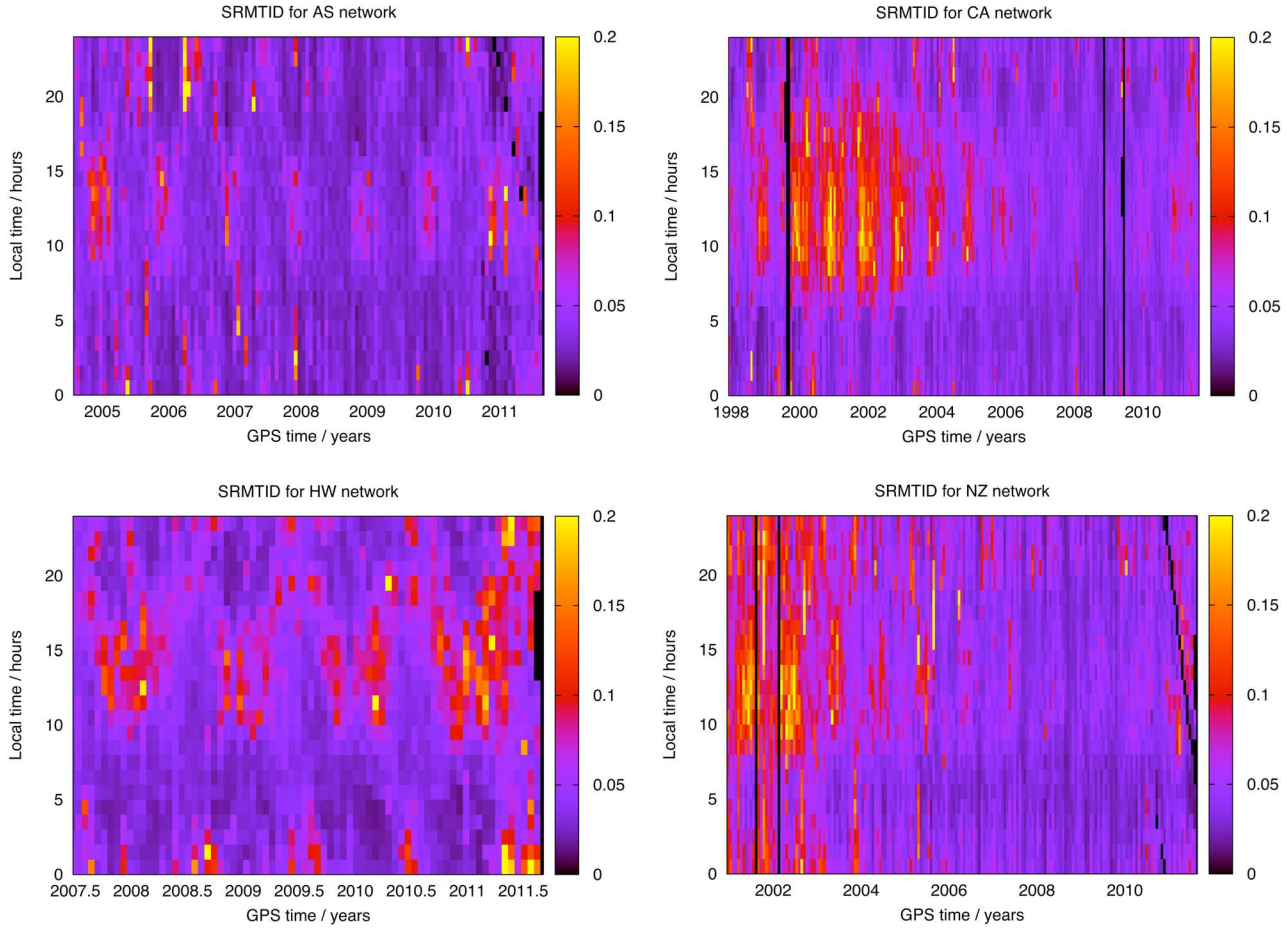

Figure 8. SRMTID index (in TECUs), in terms of GPS time (x-axis) and local time (y-axis), for the four selected networks: (top left) AS, (top right) CA, (bottom left) HW, and (bottom right) NZ.

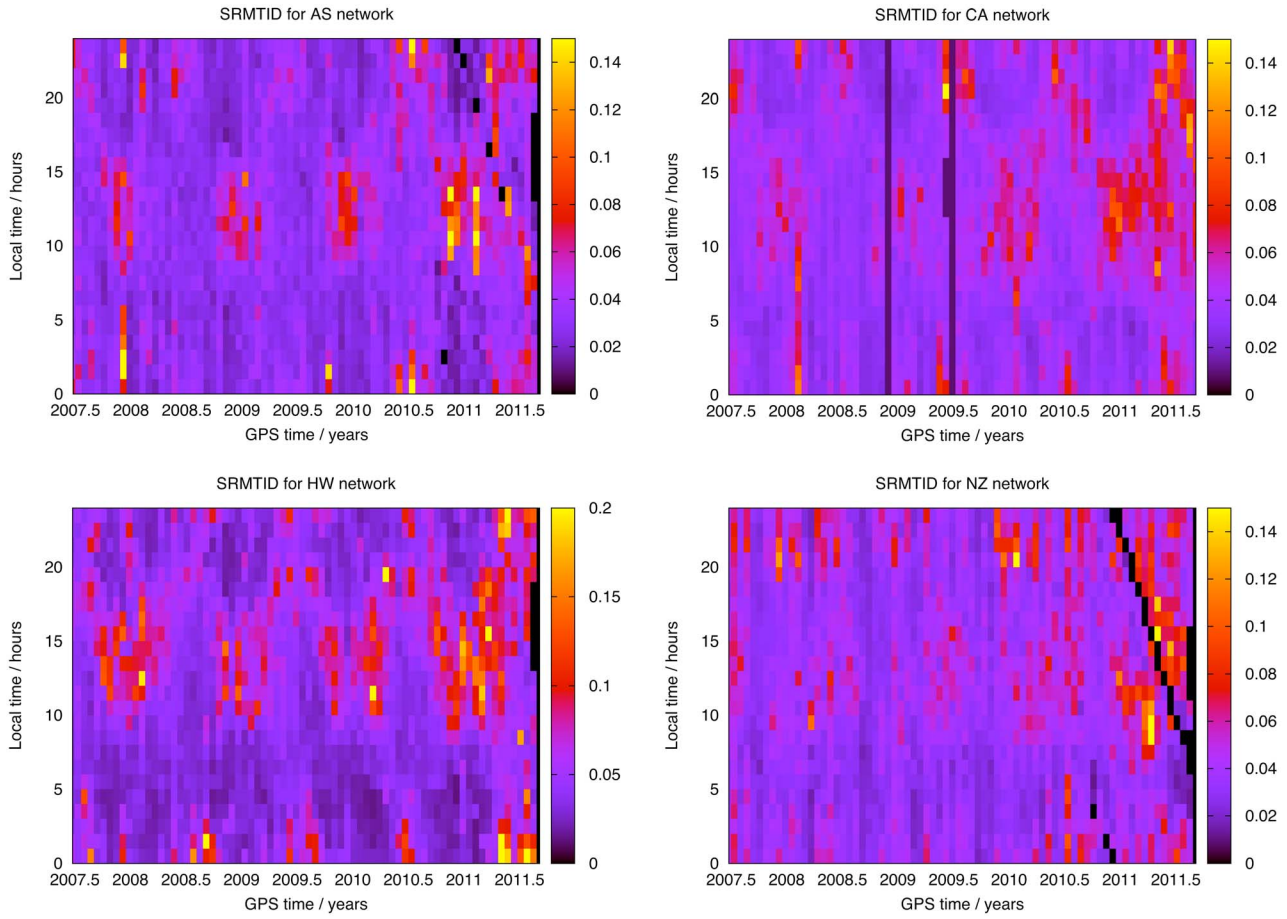

Figure 9. SRMTID index (in TECUs), in terms of GPS time (x-axis) and local time (y-axis), for the four selected networks and a common temporal window: (top left) AS, (top right) CA, (bottom left) HW, and (bottom right) NZ.

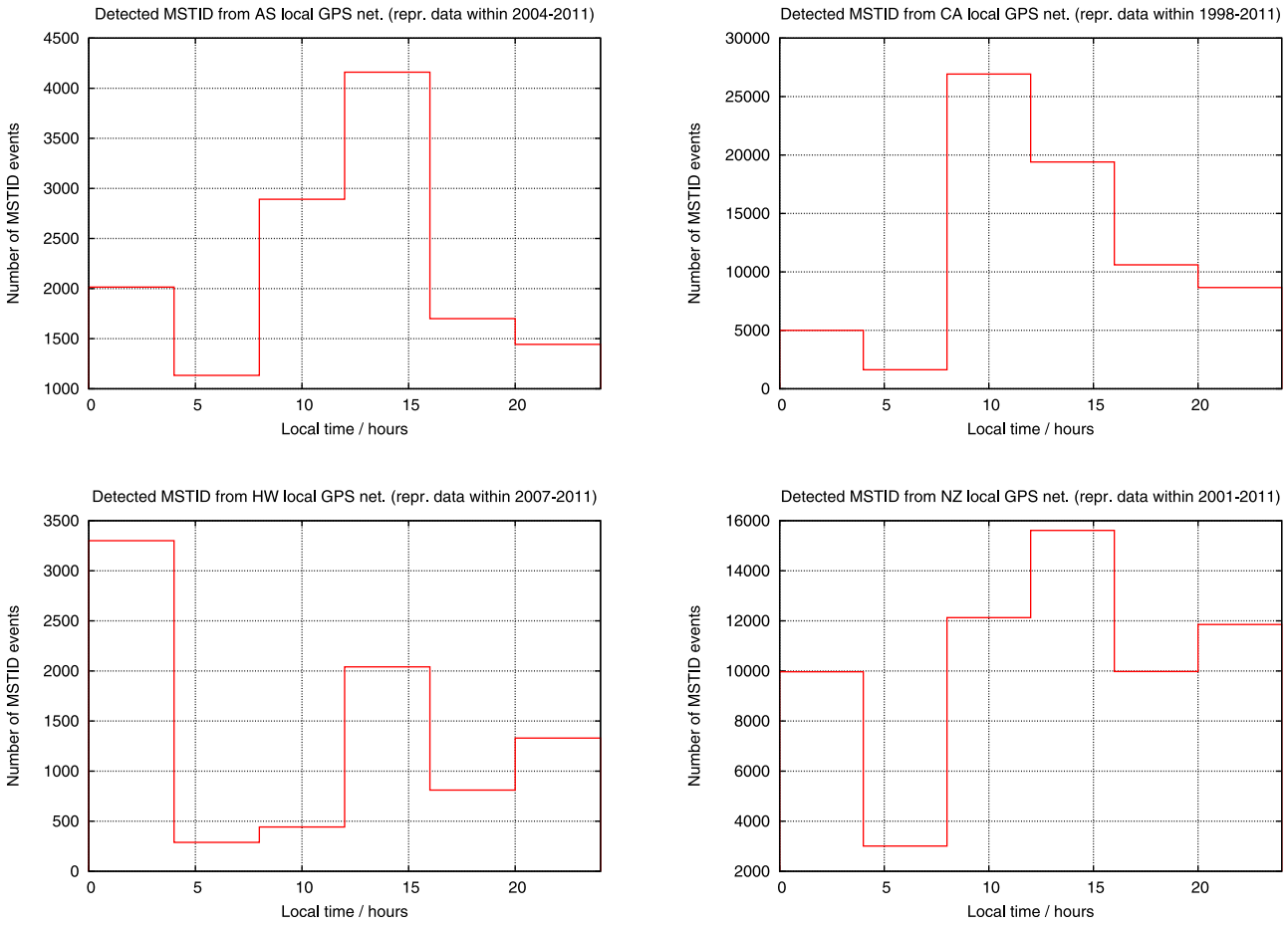

Figure 10. Number of observed MSTID events, in terms of local time (in hours), for the four selected networks and a common temporal window: (top left) AS, (top right) CA, (bottom left) HW, and (bottom right) NZ.

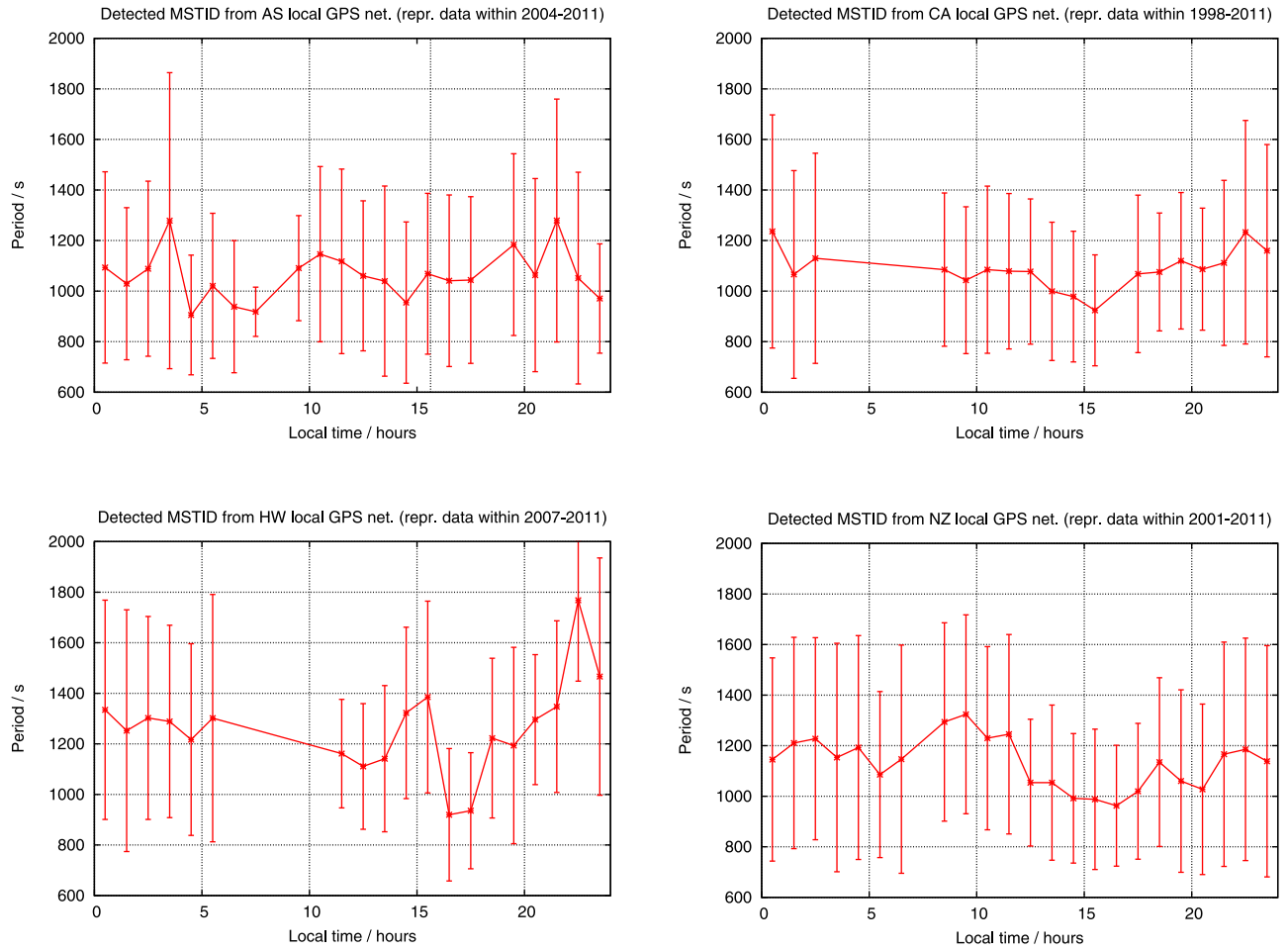

Figure 11. Mean period (points) and standard deviation (vertical bars) of the MSTID events (in seconds), in terms of local time (in hours), for the four selected networks and a common temporal window: (top left) AS, (top right) CA, (bottom left) HW, and (bottom right) NZ.

introduced for each satellite in HJS06), $\mathcal{S}_{\mathcal{M}}$. It is defined as the Root Mean Squared (RMS) of the detrended Vertical TEC (VTEC) $\tilde{V}$, using a time step of τ = 300 s:

$$\mathcal{S}_{\mathcal{M}} = \sqrt{\frac{1}{N_s}\sum_{i=1}^{N_s} \tilde{V}_i^2}, \tag{4}$$

where

$$\tilde{V} \equiv \frac{\tilde{S}}{M} \tag{5}$$

is a proxy for the detrended VTEC value, M is the corresponding deprojection factor (known as mapping function) for the epoch of the central observation involved in the double difference in time and N_s is the number of satellites in view from the given receiver.

[19] The usage of $\mathcal{S}_{\mathcal{M}}$ index as MSTID activity tracer (not only for mid, but also for high and low latitudes) is supported by Figures 6 and 7, where the remarkable correlation between the SRMTID index and the module of predominant Fourier mode of $\tilde{V}$ is shown. This analysis is performed for the four studied networks, in terms of GPS time (in horizontal axis when data available, since 1998 until September 2011) and local time (vertical axis).

[20] The SRMTID index presents some advantages with respect previous indices: (1) it can be computed for isolated receivers (which is not the case for the I95 and I95L indices based on differences between receivers [*Wanninger*, 2004], and (2) it directly gives a proxy of the magnitude of the averaged MSTID amplitude (with the corresponding filter factor, see Figure 5), which is the magnitude affecting to several applications (instead of the normalized standard deviation of TEC perturbations within 1 hour, as used in *Tsugawa et al.* [2007], or the normalized perturbations in the F2 layer electron density peak as used for instance in *MacDougall and Jayachandran* [2011]).

3.3. Determination of Propagation Parameters

[21] To determine the MSTID propagation parameters, the ionospheric carrier phase measurements, L_I, of the GPS satellites, simultaneously observed from the local network receivers are used, to get the band pass filtered STECs $\tilde{S}$, as explained before. From this point two steps have been

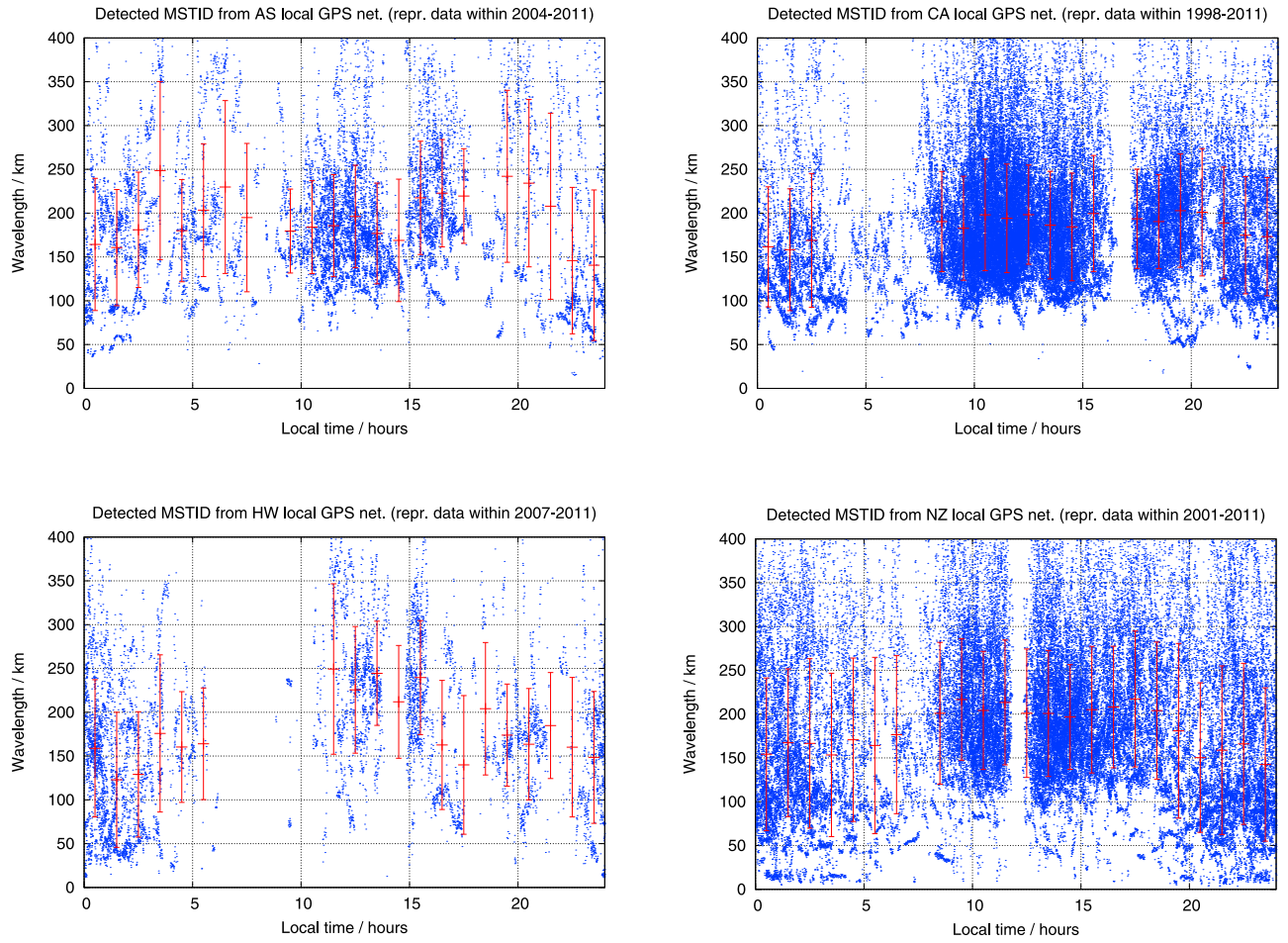

Figure 12. Mean wavelength (points) and standard deviation (vertical bars) of the MSTID events (in km), in terms of local time (in hours), for the four selected networks and a common temporal window: (top left) AS, (top right) CA, (bottom left) HW, and (bottom right) NZ.

followed for each given GPS satellite in view from the local network:

[22] 1. To obtain the time delay Δt_i of the main MSTID signal by each receiver, relative to the corresponding observation from a reference receiver.

[23] 2. To estimate the horizontal propagation velocity, for a given epoch, from the different time delay values $\{\Delta t_i\}_{i=1,Ns}$, under the assumption of a planar wave behavior of the MSTID at the local network length scale of few tens of kilometers.

[24] Indeed, for a given signal $\tilde{V}$ measured in the time domain, its Fourier transform $\mathcal{F}\{\tilde{V}\}$ in the frequency domain can be defined as (following for instance *Press et al.* [1992]):

$$\mathcal{F}\{\tilde{V}\}(f) \equiv \int_{-\infty}^{+\infty} \tilde{V}(t) e^{j2\pi ft} dt \tag{6}$$

[25] Assuming a second temporal signal $\tilde{V}_{\Delta t}$, equal to the first one $\tilde{V}$ just shifted in time Δt, i.e.,

$$\tilde{V}_{\Delta t}(t) \equiv \tilde{V}(t - \Delta t), \tag{7}$$

its Fourier Transform becomes:

$$\mathcal{F}\{\tilde{V}_{\Delta t}\}(f) = \int_{-\infty}^{+\infty} \tilde{V}(t - \Delta t) e^{j2\pi ft} dt = e^{j2\pi f \Delta t} \mathcal{F}\{\tilde{V}\}(f) \tag{8}$$

by applying a change of integration variable ($t' = t - \Delta t$). In short, assuming that the MSTID behaves as a plane wave at scales of tens of kilometers, the phase delay for a given mode (such as the one carrying more signal) can be simply deduced from the difference of the corresponding Fourier coefficient complex phase. This is the so-called phase difference method, very suitable for the present study involving mass data processing, with respect correlation process used in previous works, more computationally expensive. Moreover, the phase difference method, working with the mode (or modes) with the highest energy, could provide some advantages in front of the direct correlation of the filtered signals, when several interfering modes are present in the MSTID [see *Ratovsky et al.*, 2008].

[26] Indeed, considering the detrended VTEC values $\tilde{V}$ and performing their Discrete Fourier Transform by using the Fast Fourier Transform algorithm (with a sliding window

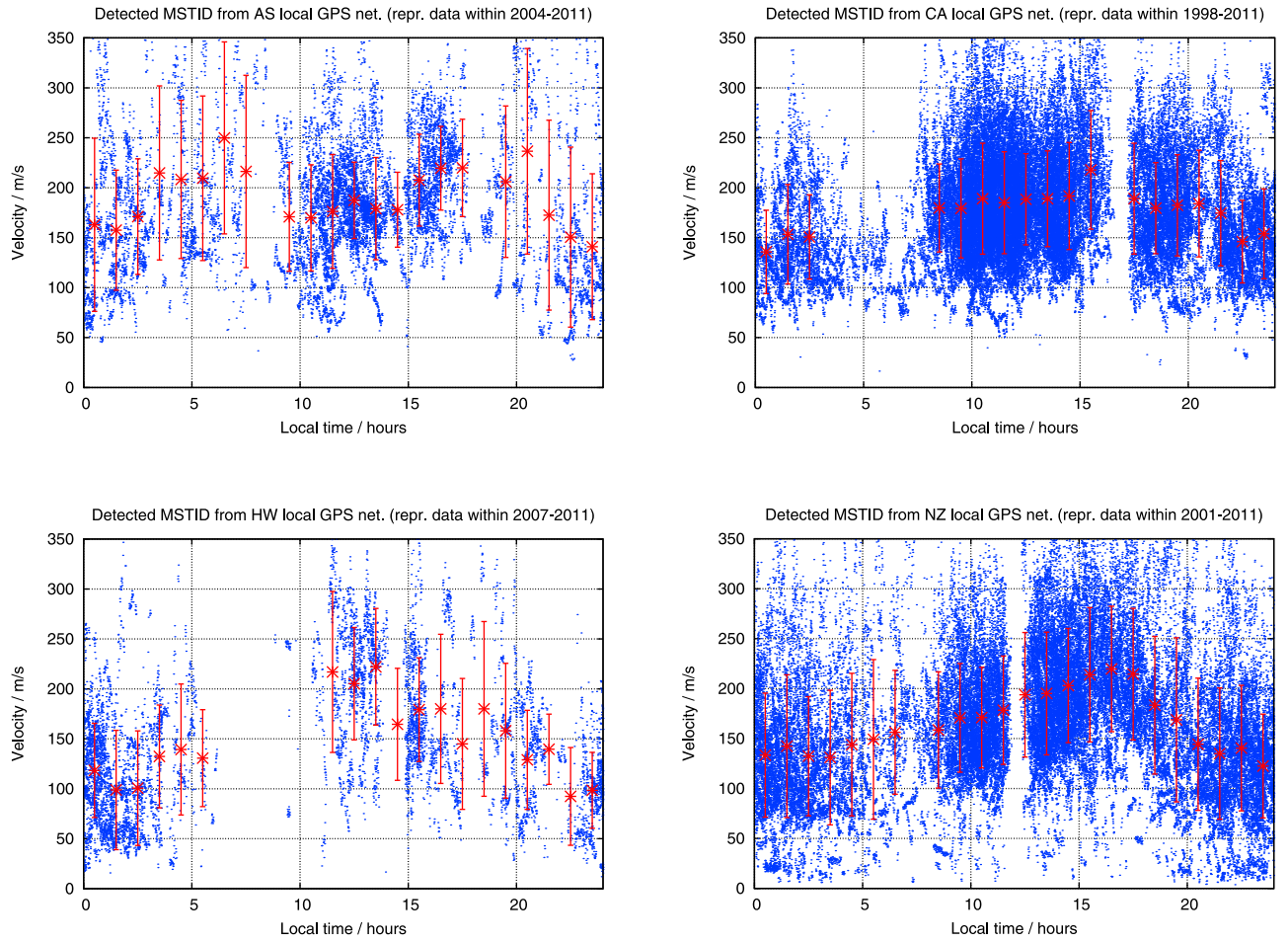

Figure 13. Mean module (points) and standard deviation (vertical bars) of the MSTID propagation velocity (in m/s), in terms of local time, for the four selected networks and a common temporal window: (top left) AS, (top right) CA, (bottom left) HW, and (bottom right) NZ.

of 64 min suitable for MSTID filtering and with $n = 2^7 = 128$ samples [see *Press et al.*, 1992]), the dominant frequency mode f_m, with higher amplitude, can be identified. When this dominant mode, for a given GPS satellite tracked from a given local network, is shared between the reference receiver and at least two receivers i (in fact three, in order to have some redundancy), the corresponding time delay Δt_i can be obtained in an straightforward way, by applying the above mentioned property of the Fourier Transform. Under this assumption the different delay values $\{\delta t_i\}$ can be used to estimate the propagation velocity.

[27] Indeed, the V planar wave phase ϕ will be dependent on the angular wave number vector $\vec{k}$ (oriented toward the propagation direction, being its module $k = \frac{2\pi}{\lambda}$, where λ stands for the wavelength), the position vector $\vec{x}$, the angular frequency $\omega = 2\pi f$ and the initial phase ϕ_0 in the well known relationship:

$$\phi = \vec{k} \cdot \vec{x} - \omega t + \phi_0 \tag{9}$$

[28] Given a MSTID affecting to the observations of a certain GPS satellite, the condition to obtain the same phase between the corresponding $\tilde{V}$ observed from two receivers of the network (i and the reference one r), can be written as:

$$\Delta\phi = \vec{k} \cdot \left(\Delta\vec{x} + \Delta\vec{x}_p\right) - \omega\Delta t = 0 \tag{10}$$

after some elapsed time Δt, with an initial difference in position $\Delta\vec{x}$, corrected with the change $\Delta\vec{x}_p = \vec{v}_p\Delta t$ of the relative ionospheric pierce position during Δt for a velocity $\vec{v}_p$.

[29] From equation (10) the key relationship to obtain the propagation velocity (equivalent to the one used in HJS06) is derived:

$$\vec{s} \cdot \vec{\beta} = 1 \tag{11}$$

where

$$\vec{\beta} = \frac{\Delta\vec{x}}{\Delta t} + \vec{v}_p \tag{12}$$

and

$$\vec{s} = \frac{\vec{k}}{w} \tag{13}$$

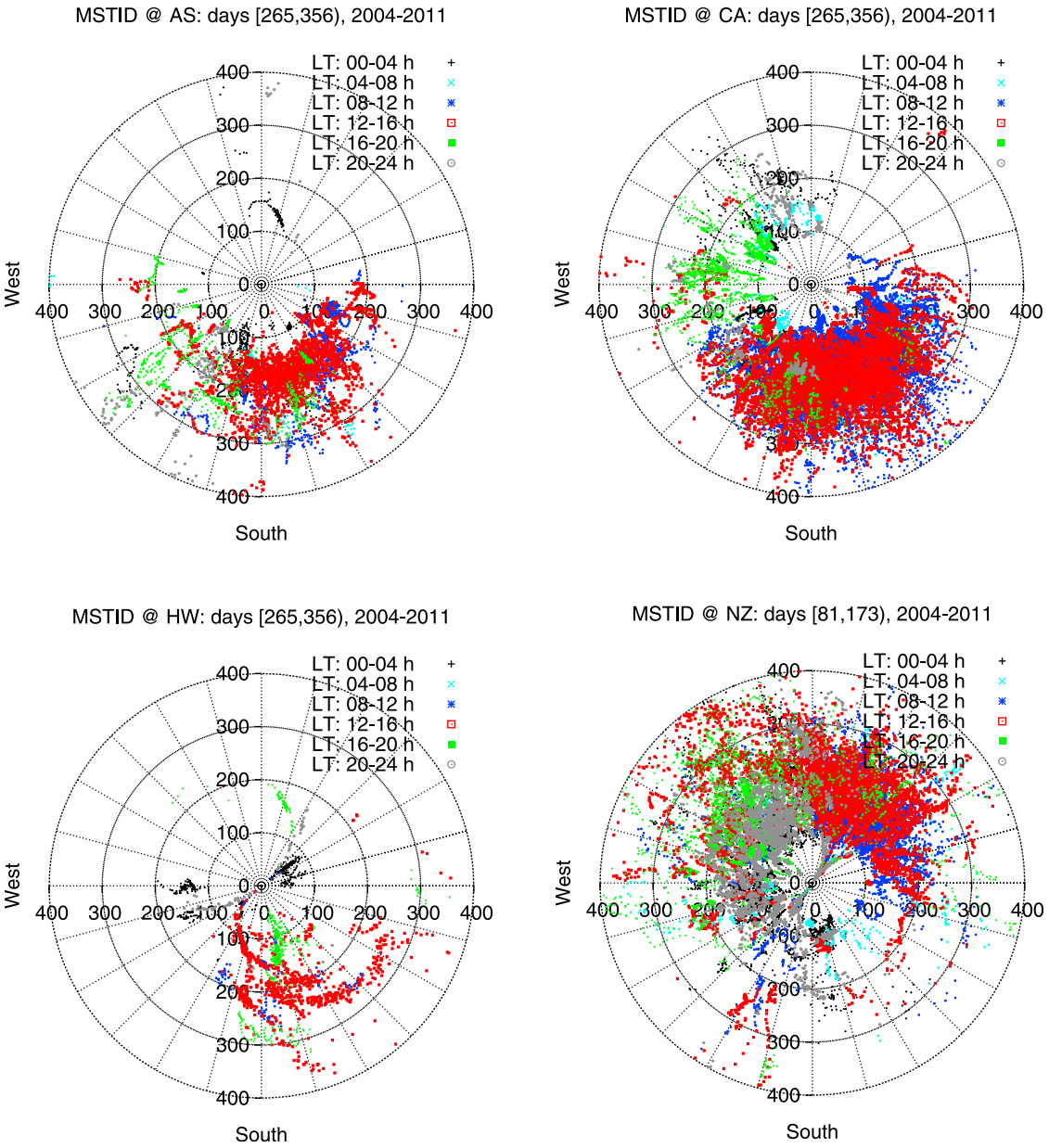

Figure 14. Polar plots representing MSTID velocities (in m/s) and azimuths for local fall, for the four selected networks, (top left) AS, (top right) CA, (bottom left) HW, and (bottom right) NZ, in the analyzed period (color palette: black for LT 00–04 h, light blue for LT 04–08 h, dark blue for LT 08–12 h, red for LT 12–16 h, green for LT 16–20 h and gray for LT 20–24 h).

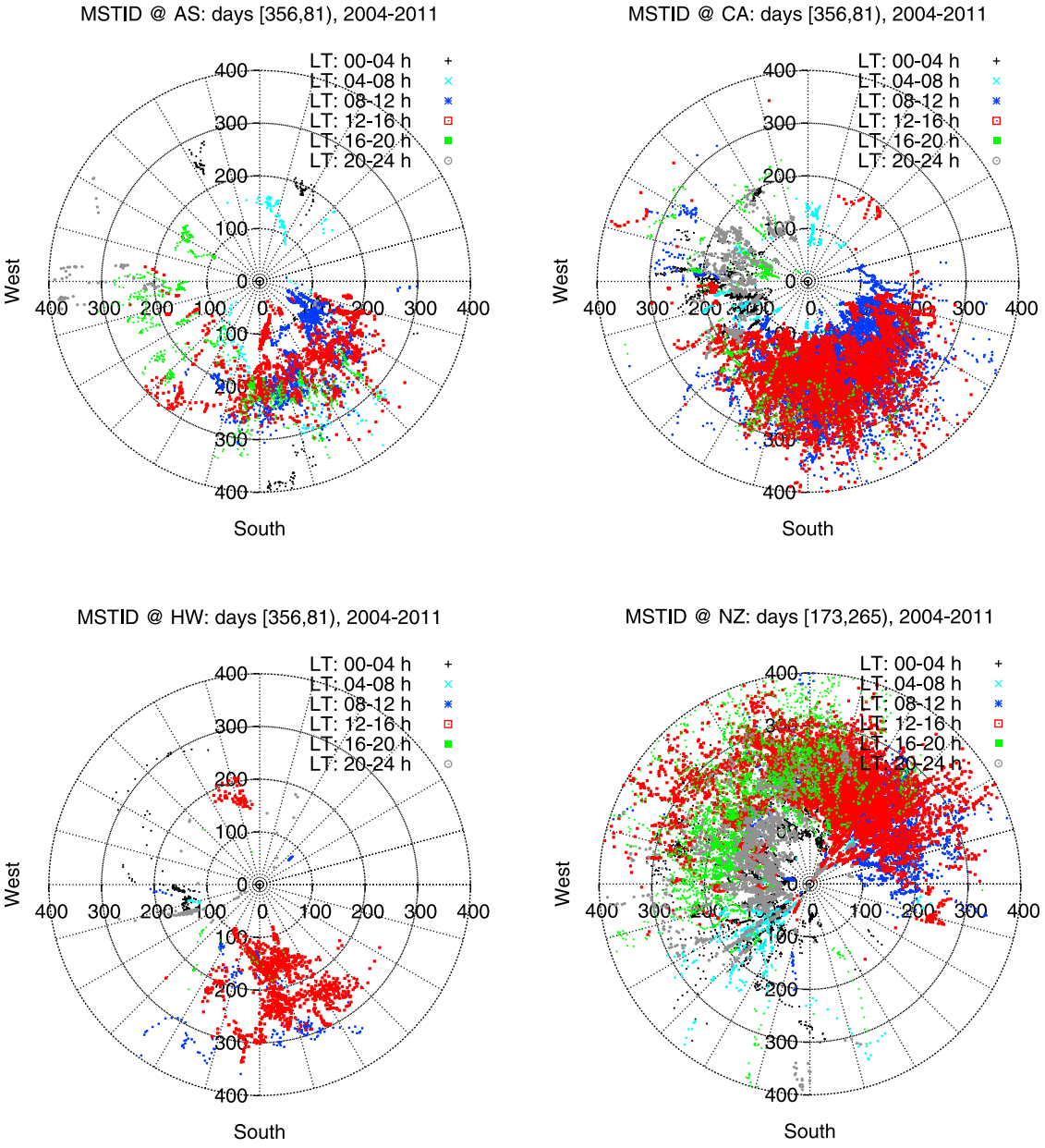

Figure 15. Polar plots representing MSTID velocities (in m/s) and azimuths, similar to Figure 14 but for local winter.

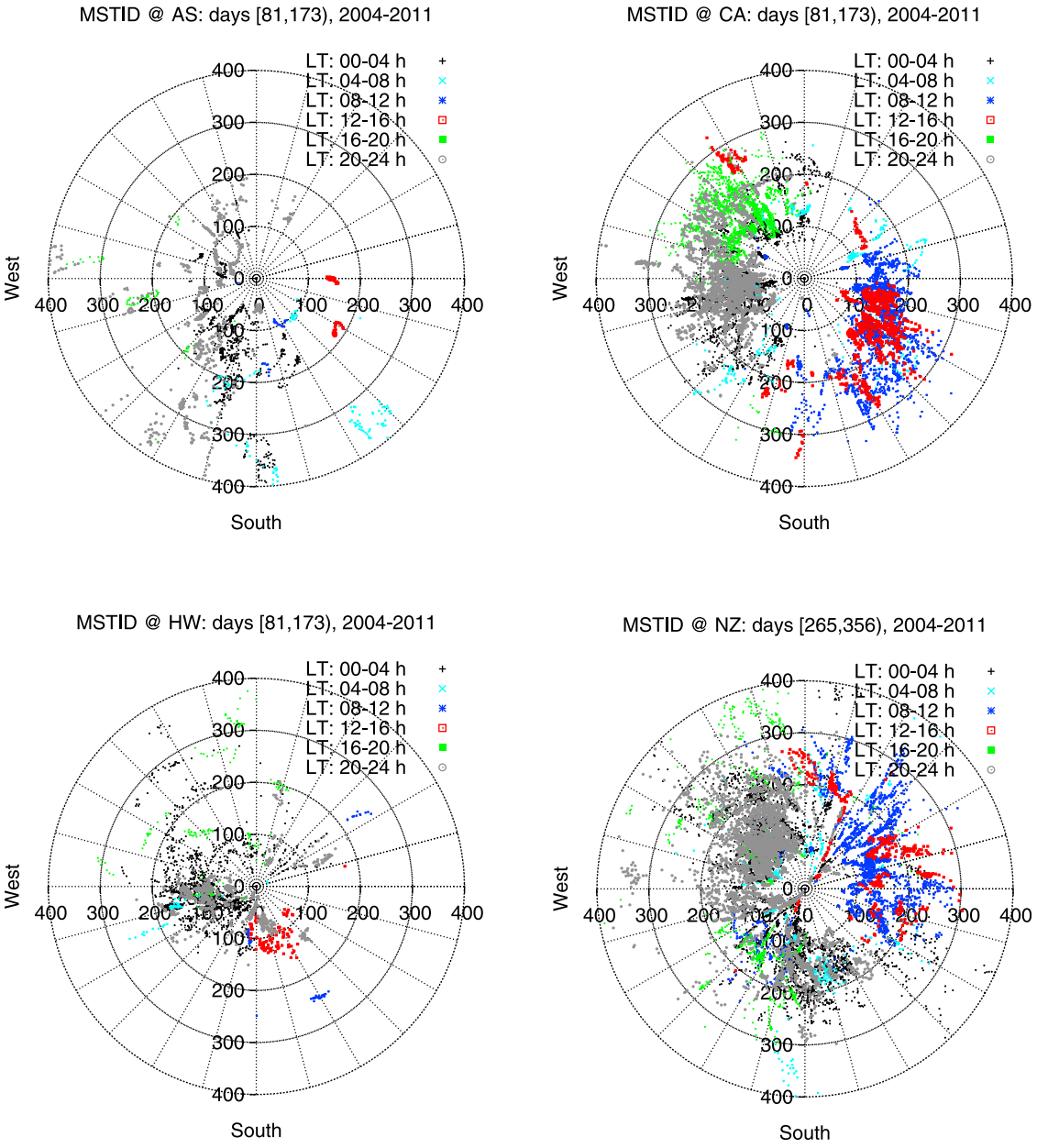

Figure 16. Polar plots representing MSTID velocities (in m/s) and azimuths, similar to Figure 14 but for local spring.

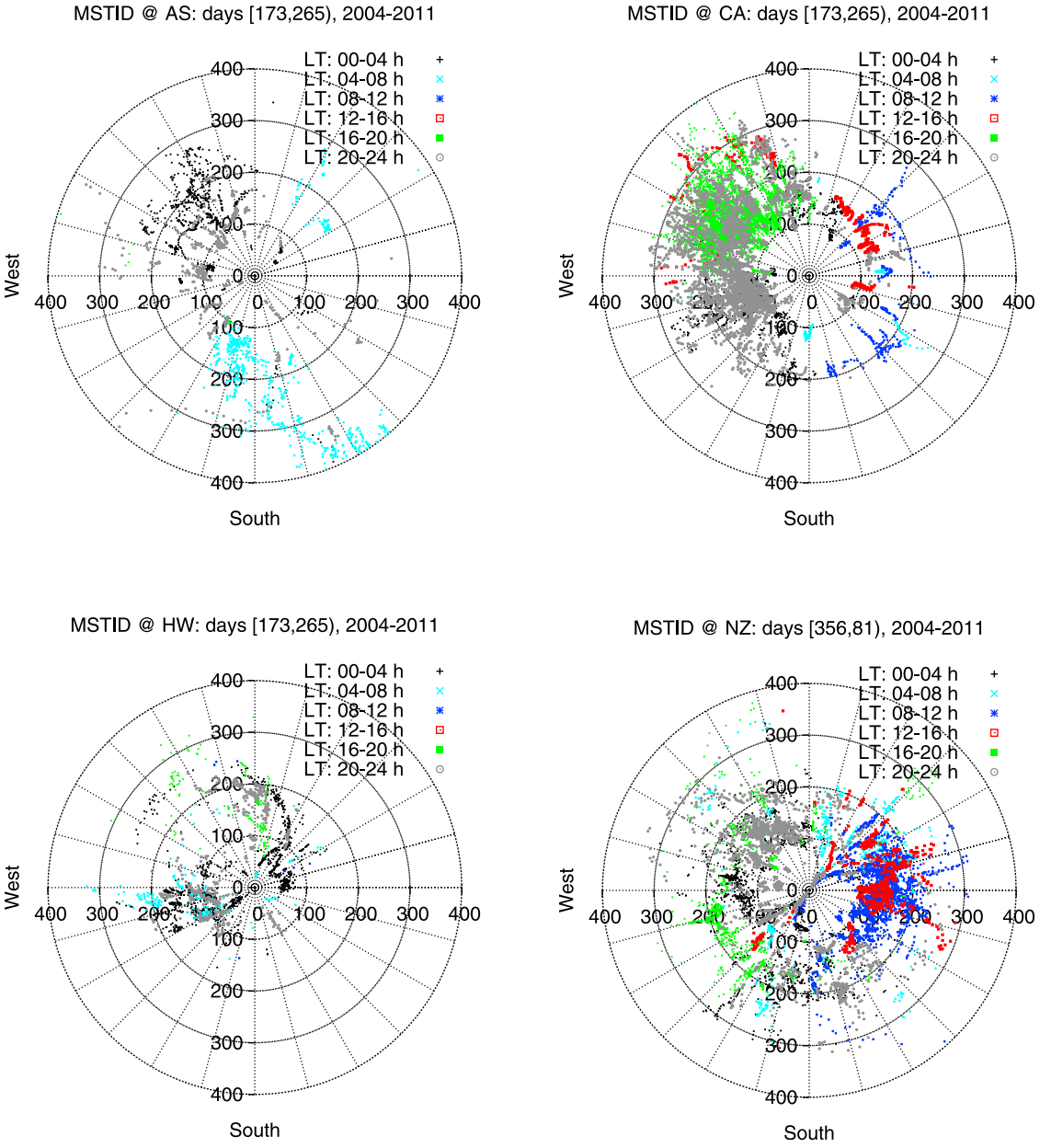

Figure 17. Polar plots representing MSTID velocities (in m/s) and azimuths, similar to Figure 14 but for local summer.

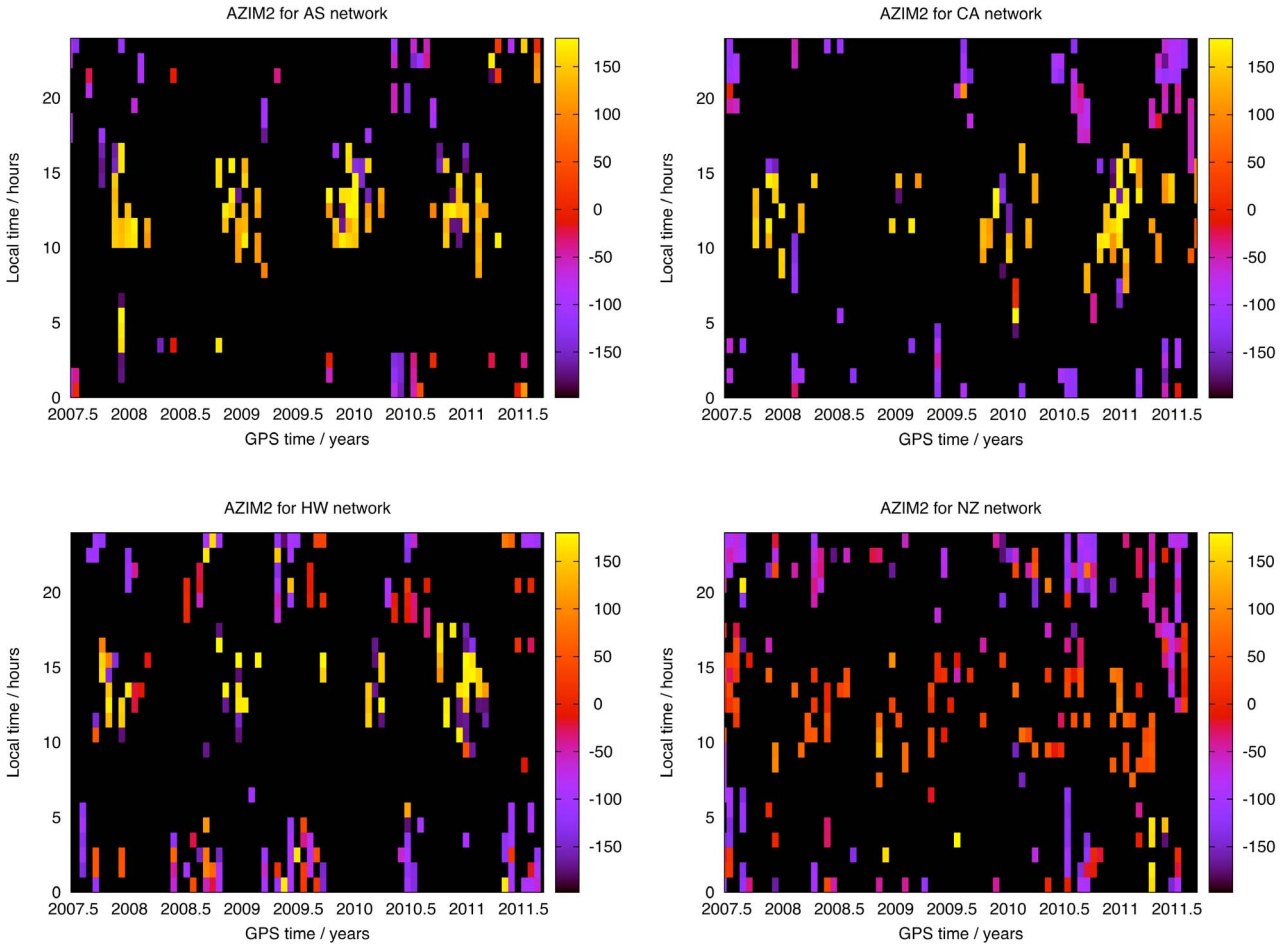

Figure 18. Propagation azimuth (from the corresponding averages of its sine and cosine to avoid the effect of rollover discontinuity), in terms of GPS time (x-axis) and local time (y-axis), for the four selected networks and a common temporal window: (top left) AS, (top right) CA, (bottom left) HW, and (bottom right) NZ.

is the *slowness* vector ($s = 1/v$). The components of $\vec{s}$ can be determined for each epoch from all the available receivers detecting a MSTID in the electron content measurements of a given satellite, with the same maximum signal mode than the reference receiver, by applying for instance the well known Least Squares Method. As the dominant geometry in the line-of-sight (LOS) of the GPS satellites observed from ground receivers is, predominantly vertical, it will be possible to mainly detect horizontal changes in the electron content. Hereinafter it will be assumed that the horizontal projection of the velocity (north and east components) will be the only component which can be directly measured (an elevation mask of 20 degrees and the usage of a mapping function makes this assumption quite acceptable, as checked by the authors). Therefore all the propagation parameters will be considered referred to the horizontal ones.

4. Resulting Characteristics of MSTIDs

[30] Applying the model summarized in section 3 to the datasets described in section 2, the following results in terms of MSTID occurrence, periods, wavelengths, velocities and azimuths have been obtained.

4.1. Occurrence

[31] It can be seen in Figure 8 that the majority of the most intense MSTID activity occurs at daytime during in fall/winter and nighttime during spring/summer, not only at mid latitudes (as it was shown in HJS06, Figure 7 of such paper), but also at low and high latitudes for all the available periods of time (from 4 to 13 consecutive years of data), modulated in intensity by the solar cycle.

[32] A more detailed comparison in occurrence between high, low and mid latitude can be seen in Figure 9 under solar minimum conditions for the common period of observations (2007–2011). On one hand, for all latitudes, the increase of MSTID activity from years 2010.5 to 2011.5 is evidenced, coinciding with the recent increase of solar flux (see Figure 4). On the other hand, in spite of the high activity values occurring at low latitude (HW network), the highest variability is found at high latitude (AS), with almost no MSTID night activity between July 2008 and April 2010, coinciding with solar flux minima (check Figure 4).

[33] The occurrence pattern at mid latitude, for both north and south hemispheres, is quite similar, except for some higher activity for NZ network at late evening. This feature

Table 1. Comparison of Main MSTID Propagation Characteristics Obtained in Different Works, Including the Present Paper[a]

Work	Data Source	Lat. Range	Dates	Season[b]	LT	Hor. Vel. (m/s)	Azim.[c]	Wavelength (km)	Sug. Origin
This paper	Local GPS net.	Mid	98–11	Wi/Fa[d]	day[d]	100–300	Eq-E	100–300+	ST?
					night	50–250	W		ST?
				Su/Sp[d]	night[d]	50–200	all W	50–250+	ST?
					day	100–250	E		ST?
		Low	07–11	Wi/Fa[d]	day[d]	100–300	Eq-E	50–300+	ST?
				Su/Sp	all	40–200+	W-Eq		ST?
		High	04–11	Wi/Fa[d]	day[d]	150–250+	Eq-E	100–300+	ST?
				Su/Sp	all	50–350+	Eq-(E/W)		ST?
KU-11	Airglow	High	01–02	all	night	∼135	EqW	-	AGW
MD-11	Ionosonde	Low	10–11	all[d]	day[d]	100–300	PoE	-	ITCZ
MDJ09	Ionosonde	High/Mid	07–09	all[d]	day[d]	∼160	E-Eq	-	MAGW, SRT
				all	night	∼300	W	-	MAGW, SRT
TS-07	Dense GPS net.	Mid	94–01	Wi[d]	day[d]	100–200	Eq-EqE	100–350	AGW
				Su/Wi[d]	night[d]	50–150	EqW	150–500	EF
HJS06	Local GPS net.	Mid	01–03	Wi[d]	day[d]	100–400	Eq	100–300+	ST
				Su[d]	night[d]	50–200	W	40–200	ST

[a]The paper acronyms used in first column are *Kubota et al.* [2011] (KU-11), *MacDougall et al.* [2011] (MD-11), *MacDougall et al.* [2009] (MDJ09), *Tsugawa et al.* [2007] (TS-07), and *Hernández-Pajares et al.* [2006a] (HJS06). On the other hand, the acronyms corresponding to the suggested origins by different authors (last column) are Atmospheric gravity waves in general (AGW), Electrodynamic forces (EF), Inter-Tropical Convergence Zone (ITCZ), Mesospheric atmospheric gravity waves due to meteorological processes (MAGW), Sun Rise Terminator (SRT) and Solar Terminator in general(ST).
[b]Season acronyms: Sp = spring, Su = summer, Fa = fall, Wi = winter.
[c]Propagation acronyms ("toward"): Eq = equator, Po = polar, E = east, W= west.
[d]High activity component.

is also noticeable in Figure 10, where the occurrence (number of detected MSTID events) only in terms of local time is shown, for MSTID events such as the module of the dominant MSTID frequency greater than 0.7 TECU (this threshold is maintained for the rest part of the study, see Figure 7). In this way it is confirmed that the most prominent occurrence is during 09–16 LT (centered at winter season) and, secondly -at mid latitude-, at nighttime, 20–24 LT (around summer time), with the exception of low latitude (HW) where the number of MSTID events is higher during 00–04 LT. In this figure a common lack of MSTID activity is also noticeable between 04 and 08 LT, which can become of potential interest for applications where MSTID is a significant nuisance.

4.2. Wave Characteristics

[34] The average discretized and apparent MSTID periods (which can be affected by the mean Doppler effect within the sliding windows of 64 min) are roughly shown in Figure 11: Most of them are distributed between 800 and 1600 s. A similar pattern can be seen for mid latitude networks at both hemispheres, with a minimum around 1000 s during 15–16 LT. The period pattern is different at low latitude (maximum of more than 1400 s before midnight).

[35] In Figure 12, only showing observations associated to significant MSTID activity, it can be seen that the typically lowest MSTID apparent wavelengths, derived from the velocities and raw periods, occur at nighttime (50–250 km, around the local summer season).

[36] The average velocities are typically in the range 50–200 m/s during local summer nighttime and 100–300 m/s during local winter at day-time (see Figure 13).

[37] The velocities and corresponding azimuths can be seen in the more detailed polar plots for fall, winter, spring and summer conditions (Figures 14–17, respectively), in terms of local time intervals of 4 hours for the four local networks. A common seasonal behavior is found between mid, high and low latitudes: Equator-eastward velocities in local daytime fall/winter seasons, about 100–300 m/s at mid latitudes, 150–250 m/s at high latitude and 100–300 m/s at low latitude (see Figure 13 as well).

[38] In summer/spring nighttime the propagation behavior is different between mid latitude (westward propagation at 50–200 m/s in both north and south hemispheres), and low -and specially high latitude, with a high dispersion of velocity and azimuth at most local times for the fewer detected events.

[39] Moreover there is a certain MSTID activity at mid latitudes propagating westward in fall/winter nighttime with velocities of 50–250 m/s, and moving eastward at 100–250 m/s in spring/summer daytime.

[40] This clear and consistent azimuth behavior is summarized in terms of day of year and local time in Figure 18 for the common time interval of 2007–2011 (the azimuth results are highly repeatable for the whole data period of up to 14 years, as in the case of the velocity distribution).

5. Discussion

[41] The main results described in previous section are summarized in Table 1, along with other recent works studying the MSTID propagation characteristics from datasets spanning at least one year, with different techniques, places and epochs.

[42] Part of the MSTID main trends found for mid, low and high latitudes during up to more than one solar cycle, confirms the main characteristics for mid latitudes reported in previous works of *Tsugawa et al.* [2007] (Japan dense GPS network) and HJS06 (Venice, Middle East local networks, CA and NZ). Indeed, this is the case for one of the main families of MSTID: It occurs in local winter (and fall) daytime, mainly showing an equatorward/equatorward-east propagation with typical velocities in 100–300 m/s range and wavelengths of 100–300 km (see Figures 15, 14, 13, and 12), in front of 100–200 m/s in *Tsugawa et al.* [2007] and

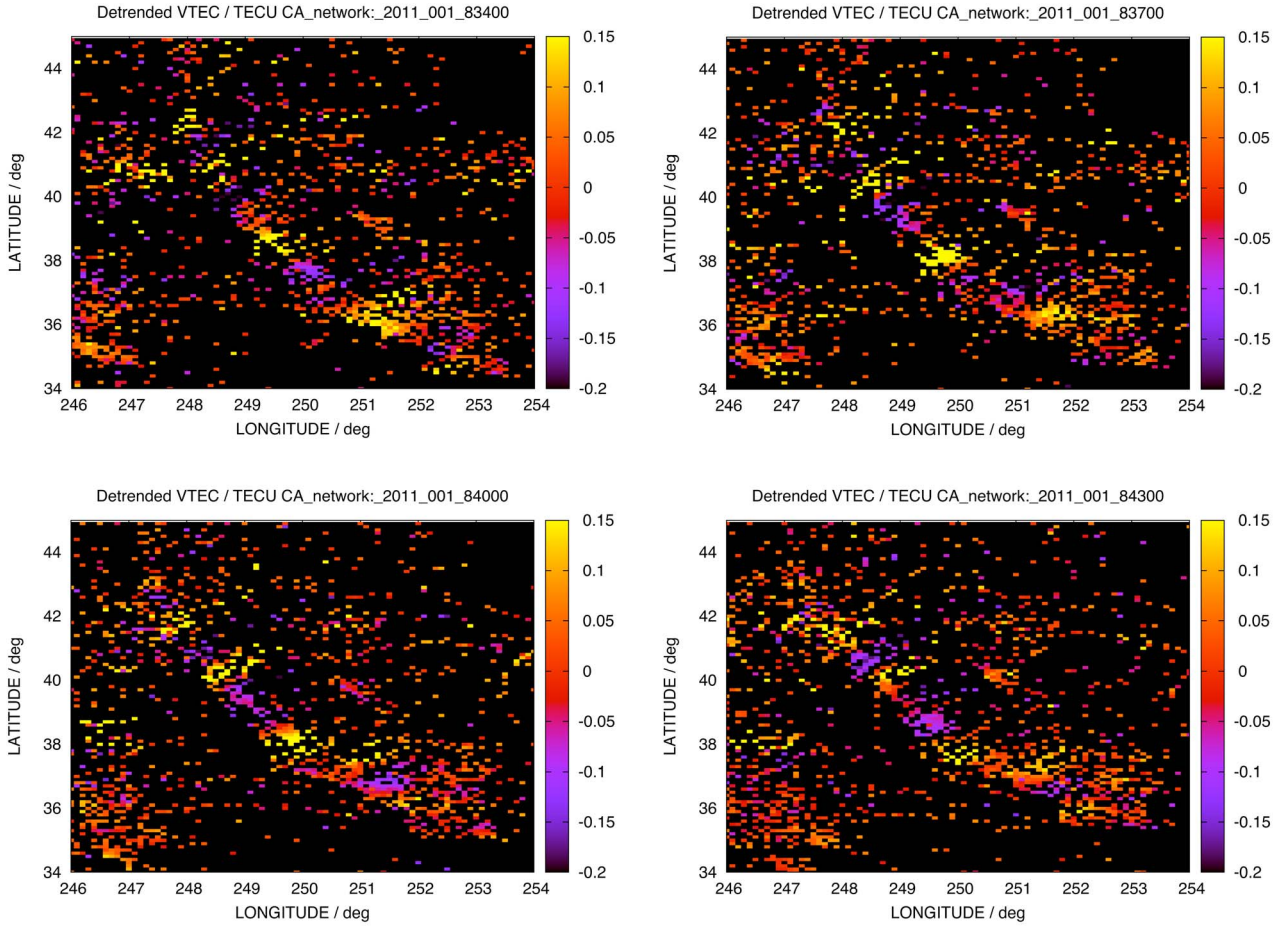

Figure 19. Daytime winter MSTID propagation fronts directly seen from detrended VTEC $\tilde{V}$ (in TECUs) over the whole dense network in California and West USA (first day of 2011, for GPS time epochs 83400, 83700, 84000 and 84300 s).

100–400 m/s in HJS06, reported for winter season. An example of this kind of wavefront propagation, in winter daytime, is depicted in Figure 19, representing $\tilde{V}$ from more than 1000 receivers in California and West USA, for four frames separated 300 s each. Compatible results are found with ionosonde data at high latitude [*MacDougall et al.*, 2009], with east-equatorward propagation at around 160 m/s, and at low latitude [*MacDougall et al.*, 2011] with velocities of 100–300 m/s. But in this case the reported propagation is poleward-east, and in both high/mid and low latitude studies (performed in Canada and Brazil with ionosonde data) there is not a clear local time pattern, contrary to the presented results during winter daytime, based on GPS data at low and high latitude sites at Hawaii and Alaska. We believe this discrepancy is related, as commented above, to the usage of different kind of MSTID activity indices between both works, absolute in this case and relative in the mentioned previous works.

[43] Regarding to local summer (and spring) nighttime, when the MSTIDs mainly travel westward with velocities of 50–200 m/s and wavelengths of 50–300 km, this is also in fully agreement with *Tsugawa et al.* [2007] and also with HJS06 (50–200 m/s) reported only for summer. Moreover a second, less frequent, MSTID propagation toward the east and at daytime, has been detected in this work, occurring also in summer (and spring), but only for mid latitude networks, at both hemispheres, CA and NZ (see Figures 17, 16, 13, and 12). Similarly some westward, nighttime activity in winter has been detected at mid latitude too.

[44] This concordance with midlatitude behavior is remarkable, in particular for low latitude network HW, in agreement with the specific low latitude MSTID study in *Lee et al.* [2008], performed with the Taiwan GPS network. In such case study, MSTID activity during local spring nighttime is reported, moving equator-westward with velocities of 100–160 m/s. However, the reported wavelength (500 km) is significantly higher than those typically obtained for similar conditions in the present paper for HW network (40–200 + km). Nevertheless we would like to stress that the winter/fall daytime behavior at low latitude is in agreement with those reported by different authors, including *MacDougall et al.* [2011], but in disagreement with one of their conclusions about the non relationship of low and mid latitude MSTID behavior, as it is shown in this work. On the other hand, recent analysis of gravity wave structures visible in noctilucent cloud images, performed in *Pautet et al.*

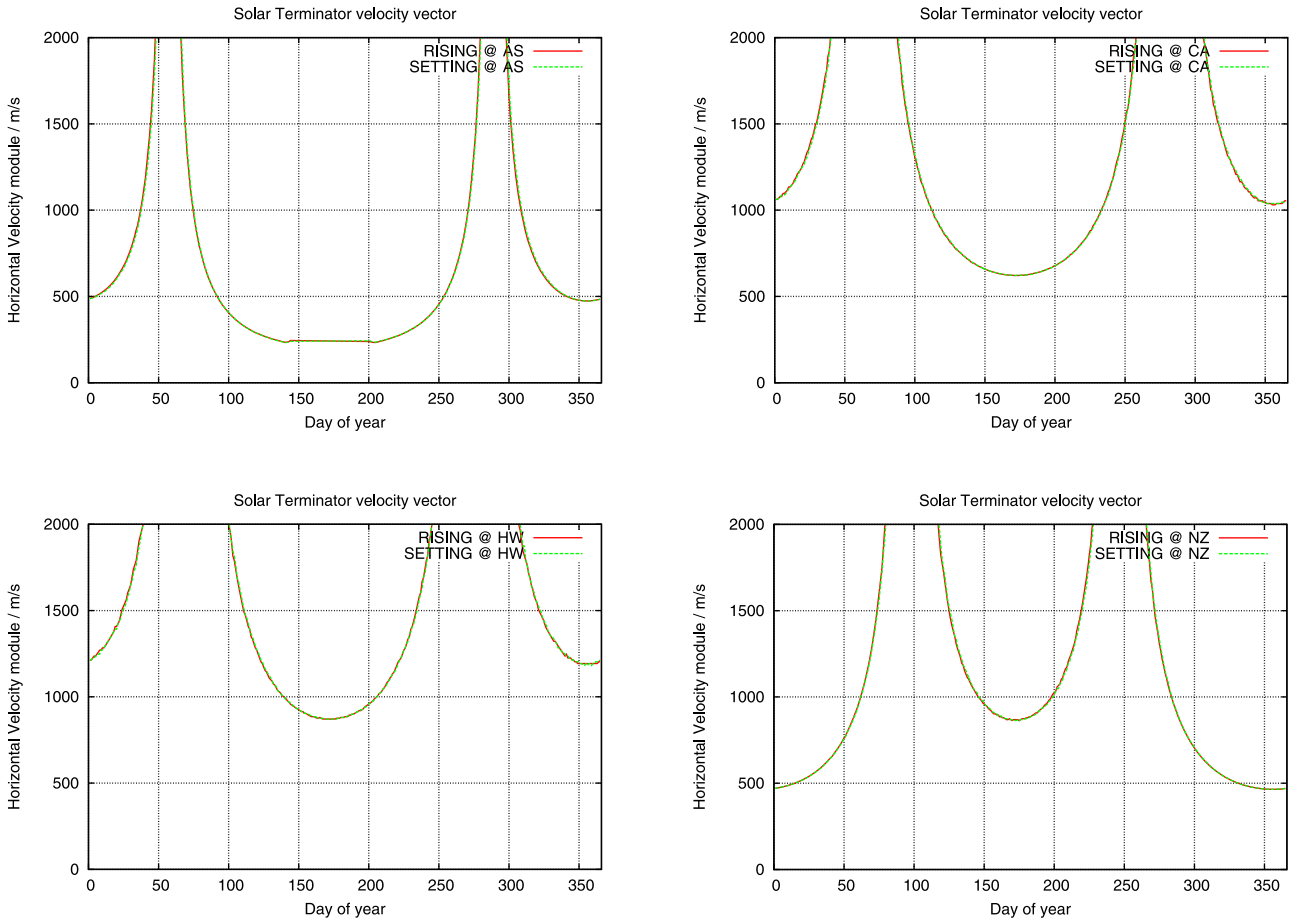

Figure 20. Module of the solar terminator horizontal velocity, in terms of the day of year (exemplarized for year 2010), for the four studied local networks: (top left) AS, (top right) CA, (bottom left) HW, and (bottom right) NZ.

[2011] during summer at high latitude (Sweden), show poleward propagation, with periods around 10–30 min. These characteristics are compatible with a noticeable pole-westward MSTID activity during summer season at high latitude, in Alaska (and also at low latitudes, see Figure 17).

[45] The main similar MSTID behavior obtained at all latitudes during fall/winter time should be considered as a significant constraint for models trying to explain its origin. Several candidate mechanisms have been proposed so far by different authors (see Table 1). Among them, the solar terminator generating Atmospheric Gravity Waves for at least daytime MSTIDs (proposed by HJS06 for both daytime and nighttime), and for night MSTIDs (the magnetic conjugate ST, hereinafter MCST, proposed by *Afraimovich et al.* [2009]), are the most supported explanations. In this regard the horizontal velocity of the solar terminator is depicted in Figure 20, as function of the day of year, for the four analyzed networks. On one hand it can be seen qualitatively that the velocities for local fall/winter are higher than the local spring/summer ones, similarly as shown for MSTIDs (this might be relevant, in line with the solar-terminator velocity dependence of the short period effect in the troposphere [see *Vasylyev and Sergeev*, 2000]). On the other hand, it can be seen in Figure 21 the overimposed ST and

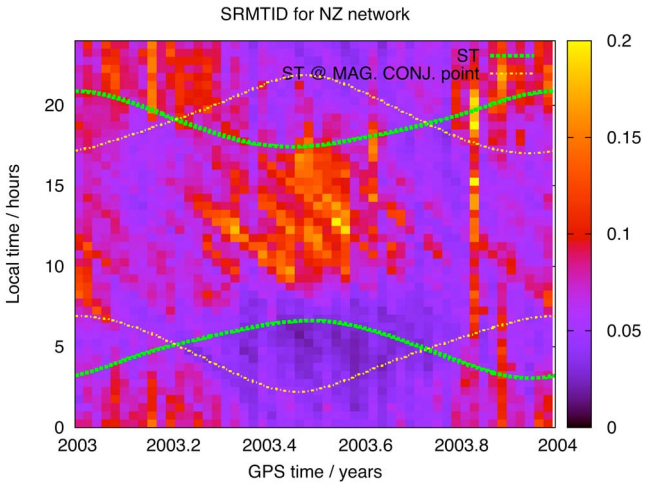

Figure 21. Occurrence of solar terminator (green thick line) and conjugate solar terminator (yellow line), in terms of the day of year, overimposed on the SRMTID index for the NZ network during the year 2003.

MCST on the MSTID occurrence (SRMTID index) in terms of GPS time and local time in more detail, for one full year of data (year 2003 of network NZ). The observed correlation, already noted in HJS06 for ST, suggests again the potential relationship with ST and/or MCST. However, another explanation for nighttime MSTIDs, alternative to ST origin (which could be compatible), pushes with force: the gravity waves at high latitudes, which would be dumped at mid latitudes, except for the Perkins direction (mostly perpendicular to the geomagnetic field [*Kelley*, 2011]).

[46] A particular aspect of the MSTID origin issue is the suggested relationship of gravity waves occurrence with E-layer activity [see, e.g., *Nygrén et al.*, 1990; *Lanchester et al.*, 1991; *Nekrasov and Shalimov*, 2002], which could be studied presently under even better conditions than in previous works such as *García-Fernández and Tsuda* [2006] (distinguishing in terms of season and local time for instance) due to the availability of many occultations (1000+ per day) provided by the COSMIC/FORMOSAT-3 constellation [see *Liou et al.*, 2007, 2010]. This can be matter of future study, by applying radio-occultation retrieval techniques [see, e.g., *Pavelyev et al.*, 2004, 2011], in particular the Improved Abel Inversion techniques much more accurate retrieving the bottom electron density [*Hernández-Pajares et al.*, 2000; *Aragon-Angel et al.*, 2011].

[47] Another future work of interest is the updating of the existing MSTID empirical models (such as the Differential Delay Mitigation MSTID Model [*Hernández-Pajares et al.*, 2006b]) with the results presented in this paper. These models can significantly mitigate the MSTID error, for instance in precise GNSS positioning (RTK or WARTK [see *Juan et al.*, 2012]) by means of a blind model (see HJS06), or, even better, by determining and broadcasting the MSTID characteristics to the users in real-time from a reduced local network providing service to wide areas (since the potential MSTID activity is independently detected and characterized for each satellite). They can also be useful to other disciplines such as Radioastronomy.

[48] **Acknowledgments.** This work has been partially supported by the Spanish Ministry of Science, Technology and Innovation under the CTM2010-21312-C03-02 project and the "Torres Quevedo" PTQ-10-03294 grant of the last author. This research has been developed coinciding with the MONITOR activity funded by the European Space Agency (ESA). The first author acknowledges to Alberto García-Rigo the data gathering of recent European datasets, used in an internal precursor study of this paper, and to Enric Monte for fruitful discussions. This work has been also possible due to the availability of the International GNSS Service data.

References

Afraimovich, E. L., I. K. Edemskiy, A. S. Leonovich, L. A. Leonovich, S. V. Voeykov, and Y. V. Yasyukevich (2009), MHD nature of nighttime MSTIDs excited by solar terminator, *Geophys. Res. Lett.*, *36*, L15106, doi:10.1029/2009GL039803.

Aragon-Angel, A., Y.-A. Liou, C.-C. Lee, B. Reinisch, M. Hernandez-Pajares, J. M. Juan, and J. Sanz (2011), Improvement of retrieved FORMOSAT-3/COSMIC electron densities validated by using Jicamarca DPS measurements. *Radio Sci.*, *46*, RS5001, doi:10.1029/2010RS004578.

Coster, A., and T. Tsugawa (2008), The impact of traveling ionospheric disturbances on global navigation satellite system services, paper presented at XXIXth General Assembly, Int. Union of Radio Sci., Chicago, Ill.

Dow, J., R. Neilan, and C. Rizos (2009), The international GNSS service in a changing landscape of global navigation satellite systems, *J. Geod.*, *83*(3–4), 191–198, doi:10.1007/s00190-008-0300-3.

Frey, S., L. Mosoni, Z. Paragi, and L. I. Gurvits (2003), Radio structure of the most distant radio-detected quasar at the ten milli-arcsecond scale, *Mon. Not. R. Astron. Soc.*, *343*, L20, doi:10.1046/j.1365-8711.2003.06869.x.

García-Fernández, M., and T. Tsuda (2006), A global distribution of sporadic E events revealed by means of CHAMP-GPS occultations, *Earth Planets Space*, *58*, 33–36.

Hernández-Pajares, M., J. M. Juan, and J. Sanz (2000), Improving the Abel inversion by adding ground GPS data to LEO radio occultations in ionospheric sounding, *Geophys. Res. Lett.*, *27*(16), 2473–2476.

Hernández-Pajares, M., J. M. Juan, and J. Sanz (2006a), Medium-scale traveling ionospheric disturbances affecting GPS measurements: Spatial and temporal analysis, *J. Geophys. Res.*, *111*, A07S11, doi:10.1029/2005JA011474.

Hernández-Pajares, M., J. M. Juan, and J. Sanz (2006b), Real time MSTIDs modelling and application to improve the precise GPS and GALILEO navigation, paper presented at ION-GNSS, Inst. of Navig., Fort Worth, Tex.

Hernández-Pajares, M., J. M. Juan, J. Sanz, A. Aragón-Àngel, A. García-Rigo, D. Salazar, and M. Escudero (2011), The ionosphere: Effects, GPS modeling and the benefits for space geodetic techniques, *J. Geod.*, *85*, 887–907, doi:10.1007/s00190-011-0508-5.

Hunsucker, R. D. (1982), Atmospheric gravity waves generated in the high-latitude ionosphere: A review, *Rev. Geophys.*, *20*(2), 293–315.

Juan, J. M., J. Sanz, M. Hernández-Pajares, J. Samson, M. Tossaint, A. Aragón-Àngel, and D. Salazar (2012), Wide Area RTK: A satellite navigation system based on precise real-time ionospheric modelling, *Radio Sci.*, *47*, RS2016, doi:10.1029/2011RS004880.

Kelley, M. C. (2011), On the origin of mesoscale TIDs at midlatitudes, *Ann. Geophys.*, *29*, 361–366.

Kubota, M., M. Conde, M. Ishii, Y. Murayama, and H. Jin (2011), Characteristics of nighttime medium-scale traveling ionospheric disturbances observed over Alaska, *J. Geophys. Res.*, *116*, A05307, doi:10.1029/2010JA016212.

Lanchester, B. S., T. Nygrén, A. Huuskonen, T. Turunen, and M. J. Jarvis (1991), Sporadic-E as a tracer for atmospheric waves, *Planet. Space Sci.*, *39*(10), 1421–1434.

Lee, C. C., Y. A. Liou, Y. Otsuka, F. D. Chu, T. K. Yeh, K. Hoshinoo, and K. Matunaga (2008), Nighttime medium-scale traveling ionospheric disturbances detected by network GPS receivers in Taiwan, *J. Geophys. Res.*, *113*, A12316, doi:10.1029/2008JA013250.

Liou, Y.-A., A. G. Pavelyev, S. F. Liu, A. A. Pavelyev, N. Yen, C. Y. Huang, and C. J. Fong (2007), FORMOSAT-3 GPS radio occultation mission: Preliminary results, *IEEE Trans. Geosci. Remote Sens.*, *45*(10), 3813–3826, doi:10.1109/TGRS.2007.903365.

Liou, Y. A., A. G. Pavelyev, S. S. Matugov, O. I. Yakovlev, and J. Wickert (2010), Radio occultation method for remote sensing of the atmosphere and ionosphere, 176 pp., I-Tech Educ. and Publ. KG, Vukovar, Croatia.

MacDougall, J., and P. T. Jayachandran (2011), Solar terminator and auroral sources for traveling ionospheric disturbances in the midlatitude F region, *J. Atmos. Sol. Terr. Phys.*, *73*, 2437–2443.

MacDougall, J. W., G. Li, and P. T. Jayachandran (2009), Traveling ionospheric disturbances near London, Canada, *J. Atmos. Sol. Terr. Phys.*, *71*, 2077–2084.

MacDougall, J., M. A. Abdu, I. Batista, R. Buriti, A. F. Medeiros, P. T. Jayachandran, and G. Borba (2011), Spaced transmitter measurements of medium scale traveling ionospheric disturbances near the equator, *Geophys. Res. Lett.*, *38*, L16806, doi:10.1029/2011GL048598.

Nekrasov, A. K., and S. L. Shalimov (2002), Nonlinear disturbances in the ionospheric E region under the action of internal gravity waves, *Cosmic Res.*, *40*(2), 129–133.

Nygrén, T., B. S. Lanchester, A. Huuskonen, L. Jalonen, T. Turunen, H. Rishbeth, and A. P. Van Eyken (1990), Interference of tidal and gravity waves in the ionosphere and an associated sporadic E-layer, *J. Atmos. Sol. Terr. Phys.*, *52*, 609–613.

Pautet, P.-D., J. Stegman, C. M. Wrasse, K. Nielsen, H. Takahashi, M. J. Taylor, K. W. Hoppel, and S. D. Eckermann (2011), Analysis of gravity waves structures visible in noctilucent cloud images, *J. Atmos. Sol. Terr. Phys.*, *73*, 2082–2090.

Pavelyev, A. G., Y.-A. Liou, and J. Wickert (2004), Diffractive vector and scalar integrals or bistatic radio-holographic remote sensing, *Radio Sci.*, *39*, RS4011, doi:10.1029/2003RS002935.

Pavelyev, A. G., K. Zhang, S. S. Matyugov, Y.-A. Liou, C. S. Wang, O. I. Yakovlev, I. A. Kucherjavenkov, and Y. Kuleshov (2011), Analytical model of bistatic reflections and radio occultation signals, *Radio Sci.*, *46*, RS1009, doi:10.1029/2010RS004434.

Press, W. H., S. A. Teukolsky, W. T. Vetterling, and B. P. Flannery (1992), *Numerical Recipes in C: The Art of Scientific Computing*, 2nd ed., 994 pp., Cambridge Univ. Press, Cambridge, U. K.

Ratovsky, K. G., A. V. Medvedev, M. V. Tolstikov, and D. S. Kushnarev (2008), Case studies of height structure of TID propagation characteristics

using cross-correlation analysis of incoherent scatter radar and DPS-4 ionosonde data, *Adv. Space Res.*, *41*, 1454–1458.
Scotto, C. (1995), Sporadic-E layer and meteorological activity, *Ann. Geofis.*, *XXXVIII*(1), 21–24.
Thompson, R. A., J. M. Moran, and G. W. Swenson Jr. (2001), *Interferometry and Synthesis in Radio Astronomy*, John Wiley, New York.
Tsugawa, T., N. Kotake, Y. Otsuka, and A. Saito (2007), Medium-scale traveling ionospheric disturbances observed by GPS receiver network in Japan: A short review, *GPS Solut.*, *11*, 139–144.
Vasylyev, V. P., and V. A. Sergeev (2000), Speed-resonant terminator wave generation in the Earth troposphere, *Earth Moon Planets*, *84*, 81–93.
Wanninger, L. (2004), Ionospheric disturbances indices for RTK and network RTK positioning, paper presented at ION-GNSS, Inst. of Navig., Long Beach, Calif.
Watts, C., J. Karle, and K. F. Dymond (2010), Three dimensional tomography of the ionosphere using a radio telescope interferometer, paper presented at 37th EPS Conference on Plasma Physics, Eur. Phys. Soc., Dublin, Ireland.